catalysts

MDPI

Article

Photocatalytic Concrete Developed by Short Seedless Hydrothermal Method for Water Purification

Marie Le Pivert [1,2] and Yamin Leprince-Wang [2,*]

[1] Université Gustave Eiffel, COSYS/ISME, F-77447 Marne-la-Vallée, France
[2] Université Gustave Eiffel, CNRS, ESYCOM, F-77454 Marne-la-Vallée, France
* Correspondence: yamin.leprince@univ-eiffel.fr

Abstract: Stormwater runoff management and treatment are significant topics for designing a sustainable city. Therefore, photocatalytic, permeable, and removable concrete is a promising solution to reduce pollution through leaching with permeable and scalable road. The objective of this work was to develop cost-effective and greener photocatalytic concretes that can be easily scaled-up, and to demonstrate their photocatalytic activities. To achieve this, seedless hydrothermal ZnO nanostructures (NSs) in 2 h were employed to functionalize a concrete surface by a soft functionalization process, avoiding overconsumption of energy and chemical products. In this work, two different concretes were studied and used for the degradation of organic dye in water. The results demonstrated the universality of the proposed functionalization process by showing similar gap values, ZnO NSs morphologies, and XRD pattern, compared to the concrete functionalized by the traditional two-step hydrothermal synthesis. The XRD results certified the presence of the ZnO Würtzite phase on the concrete surface. The synthesis feasibility was attributed to the basic pH and O^- groups' presence in concrete. Then, their photocatalytic efficiency was proved for organic dye removal in water. An almost total degradation was recorded after 5 h under artificial solar light, even after several uses, demonstrating a similar efficiency to the photocatalytic concrete functionalized by the traditional two-step synthesis.

Keywords: photocatalytic concrete; ZnO nanostructures; seedless method; water purification; photocatalysis

Citation: Le Pivert, M.; Leprince-Wang, Y. Photocatalytic Concrete Developed by Short Seedless Hydrothermal Method for Water Purification. *Catalysts* **2022**, *12*, 1620. https://doi.org/10.3390/catal12121620

Academic Editors: Gassan Hodaifa, Rafael Borja and Mha Albqmi

Received: 4 November 2022
Accepted: 4 December 2022
Published: 9 December 2022

1. Introduction

Sustainable city development is facing many problems such as the development of greener urban road [1]. Indeed, most of the road infrastructures in the city are impermeable, leading to more overflow and pollutants loading of rainwater, and less groundwater recharge [2]. Porous concrete material appears as one of the most promising ways to reduce stormwater volume and pollutant concentrations [1,3]. Therefore, effort has been made to develop photocatalytic concrete able to degrade and mineralize pollutants in the presence of sunlight [1–5].

Zinc oxide (ZnO) semiconductor nanomaterials have already shown great potential as an eco-friendly photocatalyst for environmental pollution remediation due to their ability to degrade and mineralize organic toxic pollutants into CO_2, H_2O, and other light by-products by photocatalysis under UV light or solar light [4–8]. Nevertheless, these ZnO nanomaterials are often synthesized by complex and expensive routes; therefore, their integration in road infrastructures could be difficult. Thus, the development of functionalized building materials using a low-cost process with minimal chemicals and a shorter manufacturing time is an emerging field of study [9].

Recently, in our previous work [4,5,10], ZnO nanostructures' (NSs) hydrothermal direct synthesis on paving block appeared as an interesting route to produce daily life photocatalytic materials for the urban pollution remediation. In addition, it is important to highlight that the ZnO surface functionalization may not affect the hydration reactions

of concrete and, consequently, its mechanical properties, contrarily to ZnO direct incorporation in concrete chemical formulation. Moreover, the hydrothermal method needs low processing temperature and short duration and could be easily scaled-up and adapted to different substrates [10–13]. Usually, ZnO NSs grow onto a substrate by two simple operating steps: (1) a seed layer deposition for creating ZnO nucleation sites on the substrate; (2) hydrothermal growth in the presence of zinc salt and hexamethylenetetramine (HMTA) to obtain ZnO NSs such as nanowires (NWs) or nanorods (NRs).

Nevertheless, this surface functionalization process for the permeable and removable concrete production needs to be improved. Indeed, depending on the ZnO seed layer deposition process employed, an annealing temperature from 300 °C to 500 °C is necessary, which could damage concrete. Moreover, even the ZnO seed layer deposition is known for allowing a better morphology and density control on ZnO NS growth; it also causes consumption of time and chemicals, leading to an additional cost [11].

The objective of this work was to determine and understand if permeable and removable concrete could be exempted from the seed layer deposition step and functionalized only by the second step to develop the cost-effective and greener photocatalytic concretes. Knowing that the ZnO NSs growth, in terms of morphology and gap value, could be influenced by the substrate textural properties (porosity, roughness, etc.) and surface chemistry (pH, surface functional groups, etc.), which, in turn, affect the photocatalytic activity (reactivity and availability of surface, light absorption, etc.) [5,8], in this work, two kinds of concrete with different porosity and chemical formulation were employed as substrates for ZnO NS growth. Indeed, for example, ZnO NSs' morphology could influence the ZnO total surface available for photocatalytic reaction. Moreover, the ZnO NSs' quality will define the gap value and, therefore, the light that could be absorbed and used in the photocatalytic process, and the surface reactivity. Their photocatalytic efficiency and durability for the degradation of two different organic dyes (Methyl Orange (MO) and Acid Red 14 (AR14)), whose degradation mechanisms have already been studied [14], under artificial solar light, were compared to their reference corresponding to concrete functionalized by two-step hydrothermal synthesis. The samples were thoroughly characterized by a scanning electron microscope (SEM) for nanostructure morphology investigation, ultraviolet–visible spectrophotometry for both ZnO bandgap measurements and the following organic dye photodegradation, and X-ray diffraction (XRD) for microstructures investigation.

2. Results and Discussion

2.1. Concrete Surface Characterization

2.1.1. Concrete Surface Observations and SEM Analysis

Figure 1 shows optical photography of both types of concrete samples before and after the ZnO NS growth by one-step seedless hydrothermal synthesis. We can note that the samples appeared more whitish after the synthesis. The same phenomenon was observed on the samples functionalized by two-step hydrothermal synthesis and was already attributed to the presence of very dense ZnO NSs on the samples surface, leading to diffuse light on the sample surface [4].

To further confirm the synthesis of the ZnO NSs and study the influence of the seedless effect, SEM analysis was used to examine concrete surfaces (Figure 2a). By comparing concrete surfaces with and without treatment, ZnO NSs were clearly observed on all sample surfaces with no significant modification whatever the concrete substrate and the hydrothermal route used. Only a very modest decline in density of ZnO NSs seemed to be observed on samples functionalized by simplified synthesis but could not be quantified. Due to the NSs' variety, no size information was precisely measured. The ZnO NS length was a size of the order of the micrometer, and the thickness was a size of the order of the nanometer.

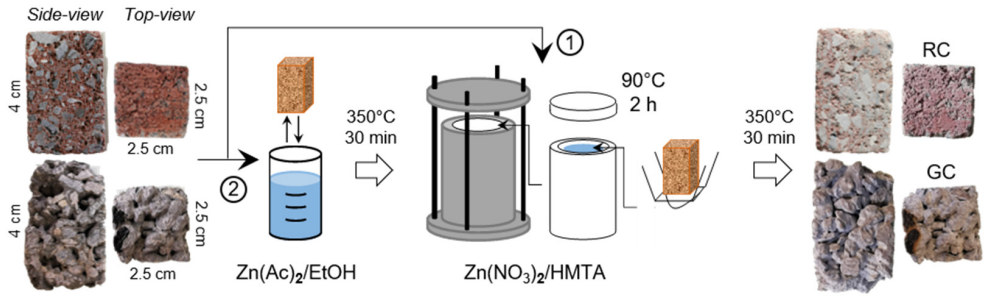

Figure 1. Schematic routes of concrete functionalization by classical hydrothermal growth in two steps (2) and seedless hydrothermal growth (1), and optical photographs of the grey concrete (GC) and red concrete (RC) blocks before and after the ZnO NS growth.

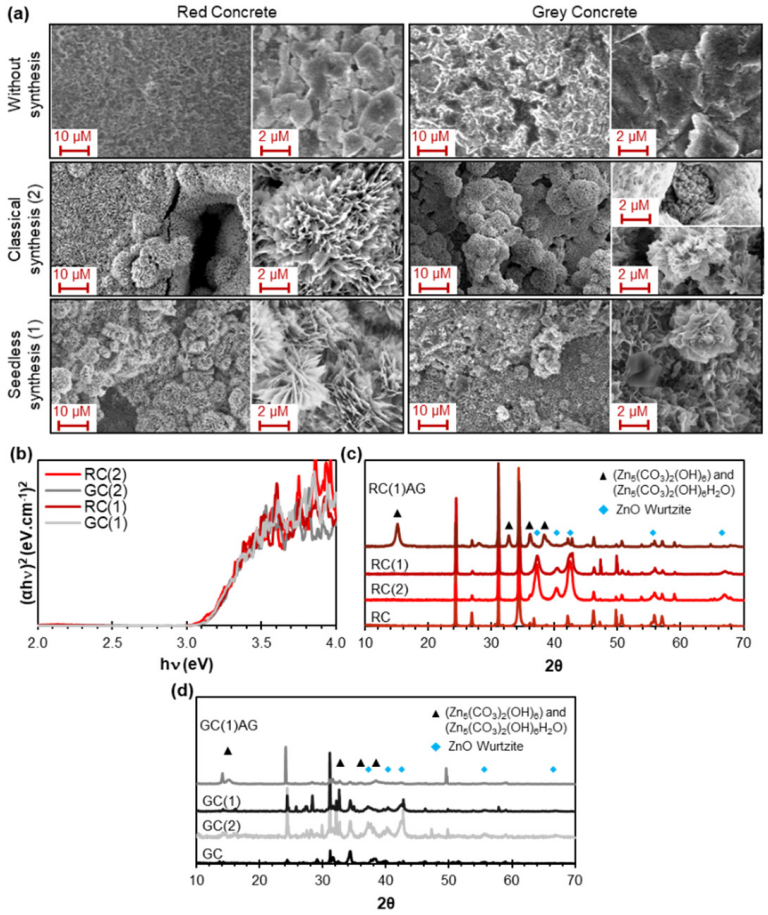

Figure 2. (**a**) SEM top-view pictures of bare concrete surfaces after 2 h of hydrothermal growth by the two-step hydrothermal method or the one-step seedless hydrothermal method; (**b**) UV-visible spectral plot with Tauc-Lorentz model of concrete surfaces after 2 h of hydrothermal growth by the two-step hydrothermal method or the one-step seedless hydrothermal method; (**c**,**d**) XRD pattern of concrete surfaces after 2 h of hydrothermal growth by the two-step hydrothermal method or the one-step seedless hydrothermal method.

However, in accordance with our previous results [5], a strong influence of the concrete complex substrate on the ZnO nanostructure growth was observed on all samples leading to complex ZnO nanostructures, such as nanosheets (NSHs), nanosheets self-assembled spheres (NSHSs), and hierarchical aggregates (HAs), instead of ZnO NWs commonly grown by this synthesis method. Indeed, on the tiling surface functionalized by route (2), ZnO NWs with an average diameter of 72 ± 10 nm and a density of 50 ± 5 NWs/µm^2 were obtained [5]. No information on ZnO NWs' length was measured on tiling, due to the

impossibility of employing the classical cleavage method for SEM cross-section observation. The ZnO NWs on concrete were only observed punctually and were larger than those obtained from tiling. This radical morphological modification was attributed to:

- The turbulence and obstruction caused by the concrete surface complex microstructure, leading to the formation of aggregates and fusion of the ZnO NSs;
- The concrete basic pH property and the chemical composition with different adjuvants used, which could act as structure-modifying agents during the hydrothermal growth [5]. Hydroxyl ions (OH^-) excess and structure-modifying agent, such as trisodium citrate ($Na_3C_6H_5O_7$), were indeed assigned to the NSHs, NSHSs, and HAs formation by being selectively adsorbed on the positively charged zinc (001) plane, leading to a total or partial suppression of growth along the (002) direction, thus favoring the growth in other directions [5,15–17].

It should be noted that no trisodium citrate was used in the formulation of GC samples [18], which, although presenting a larger diversity of ZnO morphologies, presented relatively similar ZnO NSs to RC samples (Figure 2a). Therefore, it is possible to make the following assumption: the basic pH of concrete is the main drivers in the formation of dense ZnO NSs grown as NSHs, NSHSs, and HAs instead ZnO NWs. Nevertheless, the chemical composition, the turbulence, and the obstruction effect does not have to be set aside to explain the diversity of the ZnO NS morphology.

The basic pH of concrete was also considered as the main factor allowing the ZnO NS growth on the concrete surface without needing seed layer deposition and/or metal thin film deposition, such as Au, Ag, Cu, and Sn, to assist the ZnO NSs growth [12,19–21]. The presence of excess OH^- due to the basic pH property of concrete may ensure the formation of a nucleus on the concrete surface rather than in the growth solution. It is effectively well known that OH^- plays a key role, not only in the ZnO growth mechanism by affecting the intermediate chemical reaction and facet growth direction, but also in the initial growth stage by determining the initial growth stage pathway [9,22]. At high pH, the initial growth stage pathway follows Equations (1)–(6) and is described by a quick crystal growth and a slow nucleation rate leading to several growth sites on a ZnO single nucleus, thus explaining the self-assembled structures observed on SEM images [22].

$$C_6H_{12}N_4 + 6\,H_2O \rightarrow 4\,NH_3 + 6\,HCHO \quad (1)$$

$$NH_3 + H_2O \leftrightarrow NH_4^+ + OH^- \quad (2)$$

$$[Zn(NH_3)_4]^{2+} + 2\,OH^- \rightarrow ZnO + 4\,NH_3 + H_2O \quad (3)$$

$$[Zn(NH_3)_4]^{2+} + 4\,OH^- \rightarrow [ZnO_2]^{2-} + 4\,NH_3 + H_2O \quad (4)$$

$$ZnO + 2\,OH^- \rightarrow [ZnO_2]^{2-} + H_2O \quad (5)$$

$$[ZnO_2]^{2-} + H_2O \rightarrow ZnO + 2\,OH^- \quad (6)$$

The second factor, which is assumed to be a minor factor, allowing the concrete functionalization by the seedless hydrothermal growth, is the composition of the hydrothermal growth solution. Indeed, the presence of a local OH^- excess could also be favored by the presence of NO_3^- from the zinc salt used and the presence of NH_4 from HMTA thermal decomposition. The presence of NO_3^- could accelerate the Portlandite ($Ca(OH)_2$) dissolution thanks to its affinity with Ca^{2+}, with which it will react first to form $Ca(NO_3)_2$ before being resolved in solution due to its high solubility. In the literature, concentrated ammonium nitrate in DI water (~6 mol/L) is indeed used to study the accelerated concrete leaching processes over several weeks instead of several years in reality [23]. Nevertheless, regarding the low concentration (0.025 M) and the short duration (2 h), this pathway may not be the main parameter allowing the seedless hydrothermal synthesis and may not significantly damage the concrete.

In addition to the local OH^- excess in the concrete surface caused by its basic property and its reaction with hydrothermal solution, the last factor, which can allow the ZnO NSs' direct growth without seed layer deposition, is the use of additives in the concrete formulation. The presence of O^- groups from additives in the concrete formulation could contribute to the formation of the nucleus on the concrete surface rather than in the growth solution by acting as the place of nucleation for the ZnO seedless hydrothermal growth thanks to a strong adsorption of the {0001} ZnO plane on these carboxylate groups [24].

2.1.2. Gap Measurement

Optical properties were measured at room temperature using UV-visible spectrophotometry. Then, spectra were plotted with the Tauc-Lorentz model (Figure 2b). As it can be observed, all the post-annealed samples revealed an intense absorption under 400 nm corresponding to the bandgap of ZnO. Therefore, the presence of ZnO on all the post-annealed samples was confirmed and the bandgap energy of ZnO NSs was estimated. The intercept of a straight line on this linear part with the hν abscissa is the bandgap. For all functionalized concrete samples, lower ZnO NS bandgap values (~3.13 ± 0.4 eV) than traditional ones of ZnO NWs grown on a silicon substrate [25], on tiling, and on rock samples [10] (usually from 3.20 to 3.23 eV) were recorded in line with previous results on other concrete blocks studied [5]. This variation caused by the morphology modification of ZnO NSs could be associated with their crystal quality, dislocations density, impurities, size, and thickness, for instance [5,7,22]. Indeed, NSHs are supposed to contain more oxygen defects, which could reduce the bandgap by acting as an indirect donor energy level below the conduction band [21,26,27].

Relatively reproducible ZnO bandgap values were obtained on annealed concrete samples with and without seed layer deposition (Figure 2b). This last observation suggests that the removal of seed layer deposition before the hydrothermal synthesis seemed to prevent neither ZnO NSs' growth nor ZnO NSs' good-quality synthesis onto concrete surfaces. No evident gap values were obtained from the Tauc-Lorentz method on sample RC(1)AG and GC(1)AG, due to the lack of an evident gap transition on the UV-visible absorption spectrum.

2.1.3. XRD Characterization

The concrete surface composition and crystalline phase were determined by XRD (Figure 2c,d). For RC(2), RC(1), GC(2), and GC(1), the resulting peaks at 37.2°, 40.3°, 42.5°, 55.6, 66.5°, and 74.2° are assigned to ZnO Würtzite phase (100), (002), (101), (102), (110), and (103), respectively (retaliated values from ICDD NO. 98-002-9272) [28,29]. These peaks were not initially recorded on RC and GC corresponding to the non-functionalized substrates, therefore testifying the ZnO NSs synthesis by the hydrothermal method.

As expected in light of the results achieved, XRD peak intensities indicate that the preferential orientation of ZnO NSs grown on the concrete surface was not along the (002) plane as traditionally required by the hydrothermal route without modifying agents. Once again, it demonstrates the participation of the concrete substrate in the ZnO NS growth mechanism, avoiding a growth along (002) benefiting (100) and (101) planes, which are characteristic of NSs observed by SEM.

By comparing the ZnO Würtzite peaks intensity between the sample functionalized by routes (1) or (2), it is possible to observe that the intensity decreases with the seed layer suppression step (route 1). This last result could explain the impression of a very modest decline in the density of ZnO NSs, which is not quantifiable, for samples grown by route (1).

It is important to note that there is little to no ZnO Würtzite phase on the XRD pattern of RC(1)AG and GC(1)AG. As known in the literature, it confirmed the importance of the last annealing in order to obtain a good crystallinity of ZnO after the growth thanks to the possible Zn(OH)x phase and ZnO amorphous phase conversion into the ZnO Würtzite phase. This hypothesis and the participation of concrete properties in the growth mechanism seem to be proved by the apparition of new peaks in both samples related to possible

hydrozincite ($Zn_5(CO_3)_2(OH)_6$), ashoverithe ($Zn(OH)_2$), and zinc carbonate hydroxide hydrate ($Zn_5(CO_3)_2(OH)_6H_2O$) peaks. In view of these elements, the growth mechanism in the hydrothermal solution seems to involve OH^- local excess and organic carbon groups. Then, the post-annealing process serves to convert ZnO amorphous and intermediate to ZnO Würtzite. Indeed, it is well known that species such as zinc hydroxide carbonate could be converted to ZnO thanks to annealing up to 300 °C [30].

In the light of this characterization information, the seedless one-step hydrothermal synthesis allows a functionalization of concrete with ZnO NSs without significant modification compared to those grown by two-step hydrothermal synthesis. The basic pH nature and the presence of O^- groups from concrete may be the main drivers in the formation of ZnO nuclei on the concrete surface followed by a ZnO NS growth. The suppression of the last phase of annealing seems to have an effect on the amount of quality of ZnO nanostructures.

2.2. Photocatalytic Activity Evaluation

2.2.1. Methyl Orange Removal

In order to validate the photocatalytic efficiency of the ZnO NSs functionalized concrete by the one-step seedless hydrothermal synthesis, MO degradation (60 mL at 10 µM) under artificial solar light was carried out in the presence of the samples functionalized by route (1) for subsequent experimental cycles and compared to the results with the samples functionalized by route (2) considered as a reference. Indeed, as described in our previous work [4,5], ZnO NSs grown on concrete by the two-step hydrothermal synthesis (route (2)) already showed an excellent efficiency by decomposing MO under UV light and natural solar light. The irradiance of the light received by the sample was adjusted to be comparable to a sunny summer day in France (~3700 $\mu W/cm^2$). MO degradation was monitored by UV-visible spectrophotometry every 30 min for 5 h and the degradation efficiency X(%) was estimated thanks to Equation (7). The same experiments were carried out with no concrete or no light to evaluate the photolysis and the adsorption effects, respectively.

$$X(\%) = \left(\frac{A_0 - A}{A_0}\right) \times 100 \quad (7)$$

where A_0 and A, respectively, stand for the initial and actual absorption peak values at the wavelength of the maximum absorption for the studied dye (λ_{max} = 464 nm for MO and 515 nm for AR14).

As shown in Figure 3, no strong photolysis under artificial solar light (<20%) and no strong adsorption (<35%) for RC(2) were recorded after the 5 h process. After a second cycle process, the MO adsorption rate decreased to ~8%. Therefore, the MO degradation of 94.6% observed in cycle 1 in the presence of RC(2) under solar light could be mainly attributed to the photocatalytic activity of ZnO NSs. The strong adsorption decreases in RC(2) between cycle 1 and cycle 2 could explain the photocatalytic kinetic difference. After 5 h in the presence of RC(2) under solar light, the MO degradation reached 94.6%, 95.6%, 94%, 95%, 87.4%, and 90% for cycles 1 to 6, respectively. The MO degradation kinetics could be affected by the placement of the concrete under solar light. Indeed, even a slight variation in placement could induce different illuminated surface quantities, impacting the photocatalytic degradation rate. In this regard, the kinetic difference is not discussed in depth in this article. Therefore, it is possible to consider that the RC(2) photocatalytic efficiency remains relatively stable after 6 cycles with only a slight decrease of 5% compared to cycle 1.

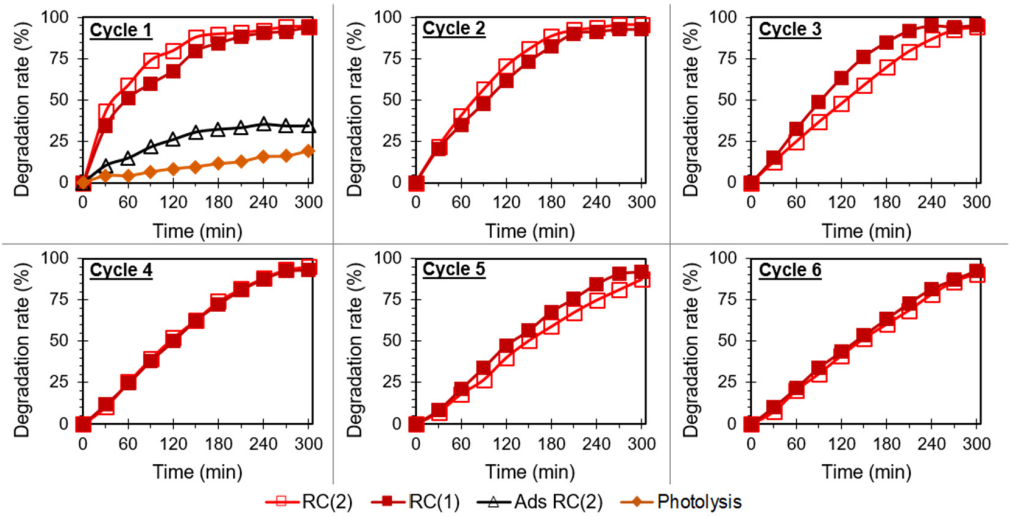

Figure 3. Photolysis degradation rate, adsorption rate in the dark (Ads), and photocatalysis degradation rate as a function of time for MO under artificial solar light in the presence of RC(2) or RC(1) for subsequent experiment cycles.

These results are promising as the stability is another important aspect in view of their application as an efficient urban depolluting surface over time. This good photocatalytic activity can be attributed to [6]:

- The fine texture of NSs and the presence of numerous boundaries increasing dye adsorption and light harvesting;
- The hierarchical structure, the various gains and interfaces facilitating the electron/hole (e^-/h^+) photogeneration, and the diffusion of e/h;
- The rich mesoporous structure helping dye adsorption and light-generated charge transfer.

By comparing the results of RC(2) with RC(1), the same trend was observed with only a small kinetic difference. After 5 h in the presence of RC(1) under solar light, the MO degradation reached 93.9%, 92.8%, 95.4%, 93%, 92%, and 92.6% for cycles 1 to 6, respectively. After several cycles, RC(1) seems slightly more stable and efficient than RC(2). Thus, it implies that the one-step seedless hydrothermal synthesis could be used to functionalize concrete surfaces with ZnO NSs as a more environmentally friendly approach to produce photocatalytic concrete for environmental pollution remediation.

To certify these observations and the universality of the synthesis process, the same experiments were carried out with the GC samples, which has a different composition and porosity than RC, as it can be seen in Figures 1 and 2c,d. In Figure 4, it is possible to note that the MO adsorption rate on GC(2) after 5 h is about 54% for the first use and about 6% for the second one, certifying that the degradation rate obtained under solar light is mainly due to the photocatalytic activity of ZnO NSs and justifying the difference in kinetics recorded between photocatalytic cycle 1 and 2. After 5 h in the presence of GC(2) under solar light, the MO degradation reached 95.7%, 94.1%, 93.7%, 91.1%, 82%, and 87.2% for cycles 1 to 6, respectively. Therefore, over 6 cycles, the GC(2) sample still provided a good photocatalytic activity comparable to RC(2) results and was relatively stable with only a slight decrease of ~9% between cycles 1 and 6.

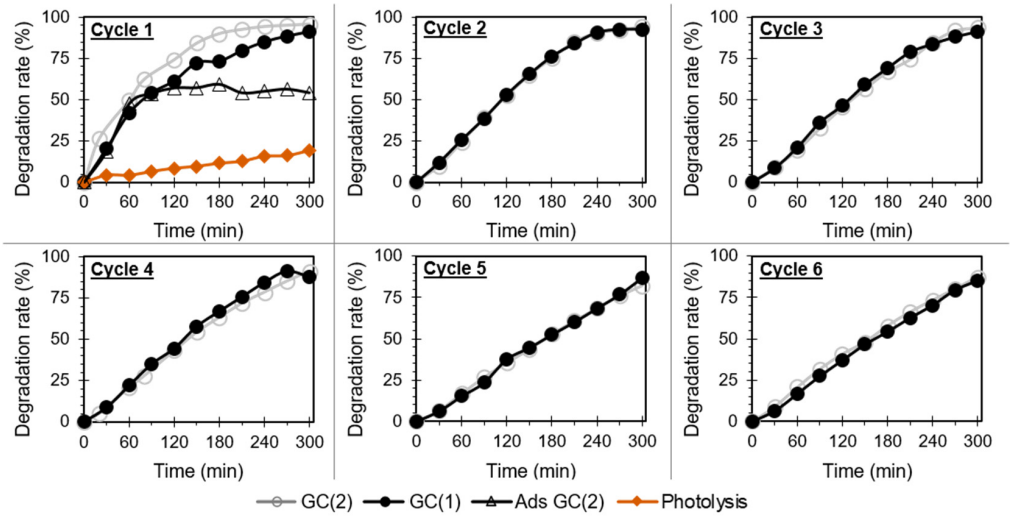

Figure 4. Photolysis degradation rate, adsorption rate in the dark (Ads), and photocatalysis degradation rate as a function of time for MO under artificial solar light in the presence of GC(2) or GC(1) for subsequent experiment cycles.

The small difference in the photocatalytic activity between GC(2) and RC(2) is likely due to the affinity and reactivity difference between MO, ZnO NSs, and the concrete. In fact, it is effectively well known that strong pollutant adsorption could be harmful for the photocatalysis depollution process by preventing water adsorption and, thus, hydroxyl radicals' creation. This variation could also be due to the porosity affecting the photocatalyst surface area, the pollutant, and light diffusion, which itself affects the photocatalytic efficiency. Indeed, photocatalytic activity could be impacted by the pollutants mass transfer from the environment to the ZnO NSs surface depending on the coupling of ZnO NSs/substrate [31].

A similar photocatalytic activity was recorded for GC(2) and GC(1) samples. After 5 h in the presence of GC(1) under solar light, the MO degradation reached 90.9%, 92.6%, 91.4%, 87.8%, 87%, and 85% for cycles 1 to 6, respectively. Therefore, the one-step seedless hydrothermal synthesis demonstrated once again its efficiency to produce more environmentally friendly ZnO-based photocatalytic concrete with similar activity and durability to those grown by two-step hydrothermal synthesis.

2.2.2. Acid Red 14 Removal

Regarding MO results, only RC(1) and GC(1) (samples obtained with seedless method), which are greener photocatalysts, were selected to conduct this study. The photocatalytic efficiency of RC(1) and GC(1) was, thus, evaluated for the degradation of another organic dye, AR14, in the same previous conditions in order to certify and compare their photocatalytic activity (Figure 5).

Their activity was proved by increasing the degradation rate ~30% after 5 h under artificial solar light compared to the photolysis degradation rate during cycle 1: 100% for RC(1), 96.3% for GC(1), and 69.2% for the photolysis. In this first cycle, it is possible to observe a sizeable difference between RC(1) and GC(1) photocatalytic kinetics, which disappeared after cycle 2. As discussed in the MO section, this initial difference could be due to the different affinity and reactivity of the pollutant with the samples and the different porosity of concrete substrates. The AR14 degradation rate after 5 h under artificial solar light for the second cycle was 100% for RC(1) and 95% for GC(1). Then, a similar slight decrease in kinetic activity both of RC(1) and GC(1) was recorded until cycle 3, leading to a degradation rate of 96.2% for RC(1) and 98.8% for GC(1) after 5 h under solar light. Beyond this cycle 3, the photocatalytic activity remained stable over time and the difference observed was mainly attributed to the error average between each cycle. The

AR14 degradation rates after 5 h under artificial solar light for cycles 3 to 5, respectively, were 99.4%, 100%, and 100% for RC(1), and 100%, 99.4%, and 97.6% for GC(1).

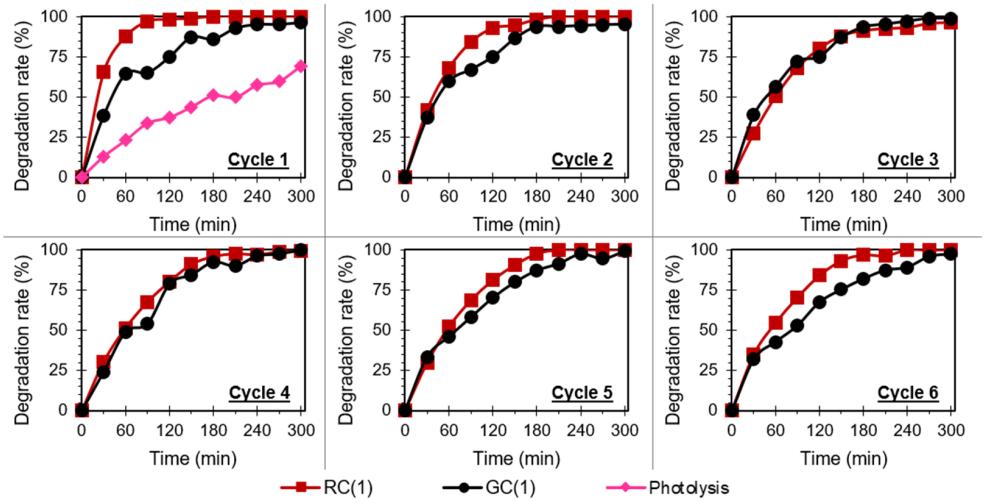

Figure 5. Photolysis degradation rate and photocatalysis degradation rate as a function of time for AR14 under artificial solar light in the presence of RC(1) or GC(1) for subsequent experiment cycles.

Despite the impossibility to make a direct comparison with previous results due to the non-identical experimental conditions, it is important to give an order of idea to the photocatalytic activity of other photocatalysts in the literature. An efficiency close to 70.4% of AR14 degradation was reached in 3.5 h with ZnO nanoparticles (60 ppm) in 50 mL of AR14-agitated solution at 20 ppm under UV-C light (30 W) [32]. A total degradation of 7 L of AR14 at 0.01 M was obtained thanks to an immobilized TiO_2 nanoparticle photocatalytic reactor, in which 7.5 mM of H_2O_2 was diffused, under a 15 W UV-C lamp in 1 h [33]. An amount of 48 mg of $ZnCo_2O_4/Co_3O_4$ eliminated 84.8% of AR14 in 65 min (1.2 mg of AR14 under 125 W of visible light) [34]. Considering photocatalytic concrete samples as fixed photocatalysts with weak weight, the results recorded are promising.

Therefore, the results from those functionalized concretes demonstrated an excellent photocatalytic activity and a relatively stable activity of samples obtained by the one-step seedless hydrothermal growth of ZnO NSs, thus illustrating that this faster and proper seedless hydrothermal growth could replace the two-step hydrothermal route for the ZnO-based photocatalytic concrete development at large scale. Nevertheless, even if this process is greener, at this stage, it still needs post-annealing at 350 °C, which may damage the substrate. For this reason and still with the objective to produce the most environmentally friendly photocatalytic concrete as possible, the post-grown annealing step of synthesis route (1) was deleted. As-grown obtained samples, RC(1)AG and GC(1)AG, were used for AR14 degradation for 3 subsequent cycles without annealing between experiments.

After 5 h under artificial solar light, the AR14 degradation rate reached 97.2%, 97%, and 96.3% for RC(1)AG from cycles 1 to 3 and 99.2%, 97.3%, and 96.2% for GC(1)AG from cycles 1 to 3 (Figure 6), respectively. The results showed that post-annealed samples and as-grown samples have similar trends and efficiency even if the amount of ZnO on the surface and its crystallinity are lower, as shown in Figure 2c,d. Only a slight drop in GC(1)AG activity could be observed and may be due to pollutants accumulation in the porous structure. It is important to note that as-grown samples were not annealed between each experiment, unlike other samples. Moreover, no other reactivation treatment, such as UV exposition, was used to replace the annealing reactivation. This last point underlines the promising application of this concrete in real life where the thermic regeneration is not possible.

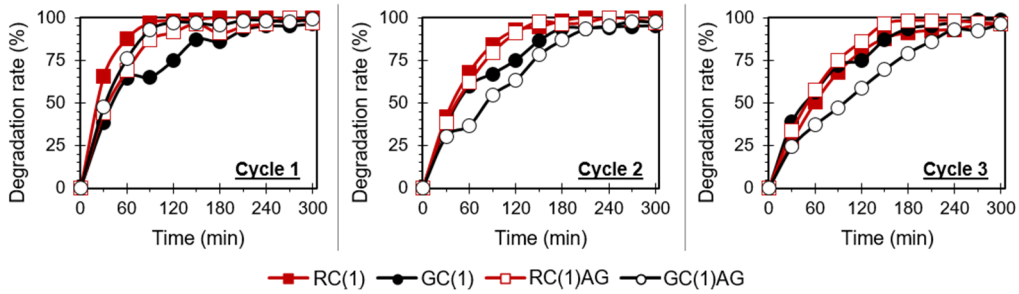

Figure 6. Photocatalysis degradation rate as a function of time for AR14 under artificial solar light in the presence of RC(1), GC(1), and RC(1)AG or GC(1)AG for 3 subsequent experimental cycles.

The results, particularly on RC samples, are very promising and put in light that it is possible to produce efficient photocatalytic concrete by only a short growth in hydrothermal solution with neither the seed layer deposition nor post-grown annealing. This method allows, therefore, a quick and low-chemical- and energy-consuming growth of ZnO NSs on concrete, which made this synthesis a very promising route for photocatalytic concrete daily life production with excellent photocatalytic activity.

3. Materials and Methods

3.1. Concrete Surface Functionalization

Red concrete blocks (purchased from DIY retailer Leroy Merlin, Lezennes, France) and grey porous concrete blocks developed by Gustave Eiffel University for a permeable and removable urban road within the I-Street/CUD-SF project (Ademe, programmes d'investissement d'avenir (PIA), France) [12] cut into pieces of ~2.5 cm × 2.5 cm × 4 cm were used as substrates for the surface functionalization (Figure 1). Prior to any synthesis, a brief washing process was first carried out on all substrates by a rinse with DI water and a drying step at 100 °C during 30 min in order to remove all dust due to the cutting step. Then, the samples were functionalized by the two different routes described below before being carefully characterized by UV-visible spectroscopy (Maya2000 Pro from Ocean Optics, Duiven, Netherlands) and by field-emission scanning electron microscopy (Zeiss FE-SEM NEON 40, Oberkochen, Germany) to determine their bandgap value and to investigate the morphology of the obtained ZnO nanostructures. The samples were also characterized by X-ray diffraction (XRD, D8 Advance, Bruker France SAS, Champs sur Marne, France) using a cobalt anticathode (λ = 1.78897 Å, 35 kV, 40 mA).

3.1.1. Two-Step Hydrothermal Synthesis Method

The two-step hydrothermal synthesis known to be efficient for functionalizing concrete surfaces was used to produce reference samples (route (2) on the Figure 1) [4,6]. First, a ZnO seed layer was deposited on a substrate by an "horizontal impregnation" method with a solution of zinc acetate dihydrate ($Zn(Ac)_2{\cdot}2\ H_2O$, 98%, Sigma-Aldrich, St. Louis, MO, USA, CAS-No 5970-45-6) at 0.01 M in absolute ethanol (99.9%, Carlo Erba, Val-de-Reuil, France, CAS-No 64-17-5) followed by an annealing at 350 °C during 30 min. Then, a classical hydrothermal growth using 300 mL of equimolar aqueous solutions of hexamethylenetetramine (HMTA, ≥99%, VWR International, Radnor, PA, USA, CAS-No 100-97-0) and zinc nitrate hexahydrate ($Zn(NO_3)_2{\cdot}6\ H_2O$, 98%, Sigma-Aldrich, St. Louis, MO, USA, CAS-No 10196-18-6) at 0.025 M was carried out in an autoclave at 90 °C for 2 h. Finally, the as-synthesized samples were annealed for 30 min at 350 °C in order to remove all potential residues from the synthesis process and to improve the ZnO NS crystallinity. The samples were named RC(2) for the red concrete functionalized with ZnO NSs or GC(2) for the grey concrete, developed for a permeable removable urban road, functionalized with ZnO NSs (see the optical photographs on Figure 1).

3.1.2. One-Step Hydrothermal Synthesis Method

This method consists of a one-step seedless hydrothermal route directly functionalizing the concrete blocks substrates. Therefore, the same hydrothermal and annealing processes as described in Section 3.1.1 were applied to the concrete substrates directly after its washing process (route (1) in Figure 1). Then, the samples were named RC(1) for the red concrete functionalized with ZnO NSs or GC(1) for the grey concrete, developed for a permeable and removable urban road, functionalized with ZnO NSs. As-grown ZnO NSs without the final annealing step were also produced for comparison and named RC(1)AG and GC(1)AG.

3.2. Photocatalytic Activity Evaluation: Water Purification

The photocatalytic activity was evaluated by the degradation of MO (85%, Sigma-Aldrich, CAS-No 547-58-0) and AR14 (50%, Sigma-Aldrich, CAS-No 3567-69-9) with an initial concentration of 10 µM under artificial solar light irradiation (Sirius 300PU, Beijing, China; 200–2500 nm; P = 5–15 sun at 50 mm from the output). The sample was immerged in 60 mL of aqueous solution polluted by MO or AR14 dye and placed under the solar source with a fixed distance of 90 cm between the lamp and the sample surface. The UV light intensity received by the sample was around ~3700 $\mu W/cm^2$ corresponding to a sunny summer day in France. In order to estimate the photocatalytic efficiency, the photolysis (without sample) and adsorption experiments in the dark were also carried out. Experiments were monitored by UV-visible spectrophotometry every 30 min for 5 h and the degradation efficiency X(%) was estimated thanks to Equation (7).

4. Conclusions

In this work, the functionalization of two different concretes (different chemical formulation and porosity) by a seedless hydrothermal growth in 2 h was studied. Their photocatalytic activity for organic dye degradation in water was investigated and compared to the concretes functionalized by traditional two-step hydrothermal growth. The results of this study showed that the seedless hydrothermal growth in 2 h could be used as a novel, faster, less expensive, and more environmentally friendly process to produce ZnO NSs-based photocatalytic concrete. Similar gap values and nanostructures morphologies were recorded for all samples functionalized whatever the concrete substrate and the hydrothermal route used. The XRD pattern demonstrated the presence of a ZnO Würtzite phase on all functionalized post-annealed samples. It is important to note that there was little to no ZnO Würtzite phase in the XRD pattern of non-post-annealed samples. No strong ZnO NSs properties modifications were recorded. It was, therefore, assumed that the basic pH and the presence of O^- groups from concrete may be the main drivers in the formation of ZnO NSs at the concrete surface without the need of seed layer deposition and/or metal thin-film deposition. The universality of this route was proved for the two different kinds of concrete.

Photocatalytic concrete from this new approach demonstrated a similar activity with the same lifetime to photocatalytic concrete functionalized by the traditional two-step synthesis in our previous work. Amounts of 85–95% of MO degradation rate and 96–100% of AR14 degradation rate were reached after 5 h under artificial solar light in the presence of functionalized concrete even after 6 cycles of use. The obtained results also showed that the post-annealed samples and the as-grown samples have a similar trend and photocatalytic efficiency.

Therefore, short seedless hydrothermal growth in 2 h can function as a very beneficial and appropriate way to develop a photocatalytic concrete surface for environmental remediation. In terms of industrial upscaling for daily life production, this short and one-step synthesis route offers a real advantage for the fabrication of photocatalytic concrete.

Nevertheless, it is important to keep in mind that this study is still a primary investigation at the initial stage. Therefore, more research should be conducted prior to use of these functionalized blocks. The ZnO NSs should be tested for resistance in traffic abrasion, dust

deposition, and other climate factors. The photocatalytic activity of aged samples should be evaluated. More in-depth research on the photocatalytic activity should be conducted to evaluate the photocatalytic activity in real conditions. The effect of the functionalization of concrete on its properties must be studied.

Author Contributions: The individual contributions was distributed as followed: conceptualization, M.L.P. and Y.L.-W.; methodology, M.L.P. and Y.L.-W.; experiments realization, M.L.P.; validation, M.L.P. and Y.L.-W.; formal analysis, M.L.P.; investigation, M.L.P.; resources, Y.L.-W.; data curation, M.L.P.; writing—original draft preparation, M.L.P.; writing—review and editing, M.L.P. and Y.L.-W.; visualization, M.L.P. and Y.L.-W.; supervision, Y.L.-W.; project administration, Y.L.-W.; funding acquisition, Y.L.-W. All authors have read and agreed to the published version of the manuscript.

Funding: This research was funded by The E3S project (2020, ANR via programmes d'investissement d'avenir (PIA), France, reference ANR-16-IDEX-0003) and the Smart Lab LABILITY of the University Gustave Eiffel (France), funded by the Region Île-de-France under Grant N°20012741.

Data Availability Statement: Not applicable.

Acknowledgments: The development of grey concrete for a permeable and removable urban road provided by Gustave Eiffel University was funded by the I-Street/CUD-SF project (Ademe, PIA). The financial and technical support linked to this project provided are gratefully acknowledged. The authors would like to thank M. Thierry Sedran and Julien Le Mouël from the University Gustave Eiffel for providing the concrete substrate and their technical help on concrete cutting. The authors would like to thank M. Nicolas Hautiére and Frédéric Bourquin from the University Gustave Eiffel for their invaluable help on this project. The authors would like to thank Myriam Duc from the University Gustave Eiffel for her helpful support to sample XRD characterization; and Stéphane Bastide from the East Paris Institute of Chemistry and Materials (ICMPE-CNRS) for his help on SEM characterization.

Conflicts of Interest: The authors declare no conflict of interest.

References

1. Liang, X.; Cui, S.; Li, H.; Abdelhady, A.; Wang, H.; Zhou, H. Removal effect on stormwater runoff pollution of porous concrete treated with nanometer titanium dioxide. *Trans. Res. Part D* **2019**, *73*, 34–45. [CrossRef]
2. Shen, S.; Burton, M.; Jobson, B.; Haselbach, L. Pervious concrete with titanium dioxide as photocatalyst compound for a greener urban road environment. *Const. Build. Mater.* **2012**, *35*, 874–883. [CrossRef]
3. Asadi, S.; Hassan, A.M.; Kevern, J.T.; Rupnow, T.D. Development of photocatalytic pervious concrete pavement for air and storm water improvements. *J. Trans. Res. Board* **2012**, *2290*, 161–167. [CrossRef]
4. Le Pivert, M.; Poupart, R.; Capochichi-Gnambodoe, M.; Martin, N.; Leprince-Wang, Y. Direct growth of ZnO nanowires on civil engineering materials: Smart materials for supported photodegradation. *Micro. Nanoengin.* **2019**, *5*, 57. [CrossRef]
5. Le Pivert, M.; Zerelli, B.; Martin, N.; Capochichi-Gnambodoe, M.; Leprince-Wang, Y. Smart ZnO decorated optimized engineering materials for water purification under natural sunlight. *Const. Build. Mater.* **2020**, *257*, 119592. [CrossRef]
6. Qiu, Y.; Wang, L.; Xu, L.; Shen, Y.; Wang, L.; Liu, Y. Shaped-controlled growth of sphere-like ZnO on modified polyester fabric in water bath. *Mater. Lett.* **2021**, *288*, 129342. [CrossRef]
7. Pastor, A.; Balbuena, J.; Cruz-Yusta, B.M.; Pavlovic, I.; Schànchez, L. ZnO on rice husk: A sustainable photocatalyst for urban air purification. *Chem. Eng. J.* **2019**, *368*, 659–667. [CrossRef]
8. Choudhary, S.; Sahu, K.; Bisht, A.; Satpati, B.; Mohapatra, S. Rapid synthesis of ZnO nanowires and nanoplates with highly enhanced photocatalytic performance. *App. Surf. Sci.* **2021**, *541*, 148484. [CrossRef]
9. Chandran, R.; Mallik, A. Facile, seedless and sufractant-free synthesis of ZnO nanostructures by wet chemical bath method and their characterization. *Appl. Nanosci.* **2018**, *8*, 1823–1830. [CrossRef]
10. Le Pivert, M.; Kerivel, O.; Zerelli, B.; Leprince-Wang, Y. ZnO nanostructures based innovative photocatalytic road for air purification. *J. Clean. Prod.* **2021**, *318*, 128447. [CrossRef]
11. Hossain, M.F.; Naka, S.; Okada, H. Fabrication of perovskite solar cells with ZnO nanostructures prepared on seedless ITO substrate. *J. Mater. Sci. Mater. Elec.* **2018**, *29*, 13864–13871. [CrossRef]
12. Hong, G.W.; Kim, J.; Lee, J.S.; Shin, K.; Jung, D.; Kim, J.H. A flexible tactile sensor using seedless hydrothermal growth of ZnO nanorods on fabrics. *J. Phys. Com.* **2020**, *4*, 045002. [CrossRef]
13. Zhang, Y.; Huang, X.; Yeom, J. A flotable piezo-photocatalytic platform based on semi-embedded ZnO nanowire array for high-performance water decontamination. *Nano-Micro Lett.* **2019**, *11*, 11. [CrossRef]
14. Habba, Y.G.; Capochichi-Gnambodoe, M.; Serairi, L.; Leprince-Wang, Y. Enhanced photocatalytic activity of ZnO nanostructure for water purification. *Phys. Status Solidi B* **2016**, *253*, 1480–1484. [CrossRef]

15. Shaban, M.; Zayed, M.; Hamdy, H. Nanostructured ZnO thin films for self-cleaning applications. *R. Soc. Chem.* **2017**, *7*, 617–631. [CrossRef]
16. Khoa, N.T.; Kim, S.W.; Thuan, D.V.; Yoo, D.H.; Kim, E.J.; Hahn, S.H. Hydrothermally controlled ZnO nanosheet self-assembled hollow spheres/hierarchical aggregates and their photocatalytic activities. *CrystEngComm* **2013**, *16*, 1344–1350. [CrossRef]
17. Luo, S.; Chen, R.; Xiang, L.; Wang, J. Hydrothermal synthesis of (001) facet highly exposed ZnO plates: A new insight into the effect of citrate. *Crystals* **2019**, *9*, 552. [CrossRef]
18. Sedran, T.; Gennesseaux, E.; Nguyen, M.-L.; Waligora, J.; Guyot, D.; Le Mouel, J. Development of a permeable removable urban pavement. In Proceedings of the International Conference on Concrete Roads, Krakow, Poland, 25–28 June 2023.
19. Wen, X.; Wu, W.; Ding, Y.; Wang, L.Z. Seedless synthesis of patterned ZnO nanowire arrays on metal thin films (Au, Ag, Cu, Sn) and their application for flexible electromechanical sensing. *J. Mater. Chem.* **2012**, *22*, 9469–9476. [CrossRef]
20. Mai, H.H.; Tran, D.H.; Janssens, E. Non-enzymatic fluorescent glucose sensor using vertically aligned ZnO nanotubes grown by a one-step, seedless hydrothermal method. *Microchim. Acta* **2019**, *186*, 245. [CrossRef]
21. Tian, J.H.; Hu, J.; Li, S.S.; Zhang, F.; Liu, J.; Shi, J.; Li, X.; Tian, Z.Q.; Chen, Y. Improved seedless hydrothermal synthesis of dense and ultralong ZnO nanowires. *Nanotechnology* **2011**, *22*, 245601. [CrossRef]
22. Adbulrahman, A.F.; Ahmed, S.M.; Hamad, S.M.; Almessiere, M.A.; Sadaji, S.M. Effect of different pH values on growth solutions for the ZnO nanostructures. *J. Phys.* **2021**, *71*, 175–189. [CrossRef]
23. Bilal, H.; Chen, T.; Ren, M.; Gao, X.; Su, A. Influence of silica fume, metakaolin & SBR latex on strength and durability performance of previous concrete. *Cons. Build. Mater.* **2021**, *275*, 122124. [CrossRef]
24. Winkler, N.; Edinger, S.; Kautek, W.; Dimopoulos, T. Mg-doped ZnO films prepared by chemical bath deposition. *J. Mater. Sci.* **2018**, *53*, 5159–5171. [CrossRef]
25. Leprince-Wang, Y.; Martin, N.; Ghozlane Habba, Y.; Le Pivert, M.; Capochichi-Gnambodoe, M. ZnO nanostructure based photocatalysis for water purification. *Nanoworld J.* **2020**, *6*, 1–6. [CrossRef]
26. Samadi, M.; Shivaee, H.A.; Pourjavadi, A.; Moshfegh, A.Z. Synergism of oxygen vacancy and carbonaceous species on enhanced photocatalytic activity of electrospun ZnO-carbon nanofibers: Charge carrier scavengers mechanism. *Appl. Catal. A Gen.* **2013**, *466*, 153–160. [CrossRef]
27. Yu, Z.; Moussa, H.; Liu, M.; Schneider, R.; Moliere, M.; Liao, H. Solution precursor plasma spray process as an alternative rapid one-step route for the development of hierarchical ZnO films for improved photocatalytic degradation. *Ceram. Int.* **2018**, *44*, 2085–2092. [CrossRef]
28. Yu, Z.; Moussa, H.; Chouchene, R.; Schneider, R.; Wang, W.; Moliere, M.; Liao, H. Tunable morphologies of ZnO films via the solution precursor plasma spray process for improved photocatalytic degradation performance. *Appl. Surf. Sci.* **2018**, *455*, 970–979. [CrossRef]
29. Joshi, S.; Jones, L.A.; Sabri, Y.M.; Bhargava, S.K.; Sunkara, M.V.; Ippolito, S.J. Facile conversion of zinc hydroxide carbonate to CaO-ZnO for selective CO_2 detection. *J. Colloid Interface Sci.* **2020**, *588*, 310–322. [CrossRef]
30. Dash, P.; Manna, A.; Mishra, N.C.; Varma, S. Synthesis and characterization of aligned ZnO nanorods for visible light photocatalysis. *Phys. E Low-Dimens. Sys. Nanostructures* **2019**, *107*, 38–46. [CrossRef]
31. Haghighat Mamaghani, A.; Haghighat, F.; Lee, C.S. Effect of titanium dioxide properties and support material on photocatalytic oxidation of indoor air pollutants. *Build. Environ.* **2021**, *189*, 107518. [CrossRef]
32. Daneshvar, N.; Salari, D.; Khataee, A.R. Photocatalytic degradation of azo dye acid red 14 in water on ZnO as an alternative catalyst to TiO_2. *J. Photochem. Photobiol. A Chem.* **2004**, *162*, 317–322. [CrossRef]
33. Mahmoodi, N.M.; Arami, M. Bulk phase degradation of acid red 14 by nanophotocatalysis using immobilize titanium(IV) oxide nanoparticles. *J. Photochem. Photobiol. A Chem.* **2006**, *182*, 60–66. [CrossRef]
34. Zinatloo-Ajabshir, S.; Heidari-Asil, S.A.; Salavati-Niasari, M. Recyclable magnetic $ZnCo_2O_4$-based ceramics nanostructure materials fabricated by simple sonochemical route for effective sunlight-driven photocatalytic degradation of organic pollution. *Ceram. Int.* **2021**, *47*, 8959–8979. [CrossRef]